

---

# Optimizing Curvature Learning for Robust Hyperbolic Deep Learning in Computer Vision

---

Ahmad Bdeir      Niels Landwehr  
Data Science Department, University of Hildesheim  
{bdeira, landwehr}@uni-hildesheim.de

## Abstract

Hyperbolic deep learning has become a growing research direction in computer vision for the unique properties afforded by the alternate embedding space. The negative curvature and exponentially growing distance metric provide a natural framework for capturing hierarchical relationships between datapoints and allowing for finer separability between their embeddings. However, these methods are still computationally expensive and prone to instability, especially when attempting to learn the negative curvature that best suits the task and the data. Current Riemannian optimizers do not account for changes in the manifold which greatly harms performance and forces lower learning rates to minimize projection errors. Our paper focuses on curvature learning by introducing an improved schema for popular learning algorithms and providing a novel normalization approach to constrain embeddings within the variable representative radius of the manifold. Additionally, we introduce a novel formulation for Riemannian AdamW, and alternative hybrid encoder techniques and foundational formulations for current convolutional hyperbolic operations, greatly reducing the computational penalty of the hyperbolic embedding space. Our approach demonstrates consistent performance improvements across both direct classification and hierarchical metric learning tasks while allowing for larger hyperbolic models.

## 1 Introduction

With the recent rise in the use of hyperbolic manifolds for deep representation learning, there is a growing need for efficient, flexible components that can fully exploit these spaces without sacrificing stability. This has led researchers to focus on two main derivations of hyperbolic space: the Poincaré manifold and the hyperboloid. The Poincaré ball, equipped with a gyrovector space, supports various well-defined operations, including generalized vector addition and multiplication, but it suffers from significant stability issues. On the other hand, the hyperboloid, or Lorentz space, lacks these operations but offers much better operation stability, as demonstrated in the study by Mishne et al. [28].

To address this gap, previous works have sought to provide Lorentzian definitions for common deep learning operations such as the feed-forward layer [3, 5, 10], convolutional layer [3, 5, 32], and MLRs [1]. This increased focus on hyperbolic modeling has led to its gradual integration into computer vision architectures, as detailed in the survey by Mettes et al. [27]. Specifically, the hyperboloid model has been employed as a sampling space for VAEs [29], a decoder space for vision tasks in hybrid settings [14, 18, 25, 31], and ultimately for fully hyperbolic Lorentzian vision encoders [1] simultaneously with its Poincaré counterpart [38].

This paper furthers the development of hyperbolic learning for vision tasks, specifically for the Lorentz manifold. Our primary focus is on the challenge of learning the manifold's negative curvature. The driving principle behind this, is that the model embeddings may exhibit varying degrees

of hyperbolicity depending on the innate hierarchies in the datapoints themselves, the problem task that is being considered, and the specific locations of hyperbolic operation integrations. To accommodate for this, we can adjust the embedding space’s hyperbolic metric to be less or more Euclidean which accounts for the modeling requirements. We also build on the idea of separate manifolds for separate main blocks in the architecture further increasing representative flexibility.

We also recognize that despite recent advances, Lorentz models continue to struggle with issues of high computational costs. We attempt to isolate and alleviate the main factors leading to numerical inaccuracies and computational overhead overall, and more particularly when modeling data in higher-dimensional embedding spaces and when learning the curvatures. Our contributions can then be summed up as:

1. We propose a formulation for Riemannian AdamW and an alternative schema for Riemannian optimizers that accounts for manifold curvature learning.
2. We propose the use of our maximum distance rescaling function to restrain hyperbolic vectors within the representative radius of accuracy afforded by the number precision, even allowing for fp16 precision.
3. We provide a more efficient convolutional layer approach that is able to leverage the highly optimized existing implementations.
4. We empirically show the effectiveness of combining these approaches using classical image classification tasks and hierarchical metric learning problems.

## 2 Related Work

**Hyperbolic Embeddings in Computer Vision** With the success of employing hyperbolic manifolds in NLP models [6, 36, 45] hyperbolic embeddings have extended to the computer vision domain. Initially, many of the works relied on a hybrid architecture, utilizing Euclidean encoders and hyperbolic decoders [27]. This was mainly due to the high computational cost of hyperbolic operations in the encoder, as well as the lack of well-defined alternatives for Euclidean operations. However, this trend has begun to shift towards the utilization of fully hyperbolic encoders as can be seen in the hyperbolic Resnets by Bdeir et al. [1] and van Spengler et al. [38]. Both works offer hyperbolic definitions for 2D convolutional layer, batch normalization layer, and an MLR for the final classification head. Bdeir et al. [1] even attempt to hybridize the encoder by employing the Lorentz manifold in blocks that exhibit higher output hyperbolicity. While this has led to notable performance improvements, both models suffer from upscaling issues. Attempting to replicate these approaches for larger datasets or bigger architectures becomes much less feasible in terms of time and memory requirements. Instead, our approach places higher focus on efficient components to leverage the beneficial hyperbolic properties of the model while minimizing the memory and computational footprint.

**Curvature Learning** Previous work in hyperbolic spaces has explored various approaches to curvature learning. In their studies, Gu et al. [13] and Giovanni et al. [12] achieve this by using a radial parametrization that implicitly models variable curvature embeddings under an explicitly defined, fixed 1-curve manifold. This method enables them to simulate K-curve hyperbolic and spherical operations under constant curvature for the mixed-curve manifold specifically, a combination of the Euclidean, spherical, and Poincaré manifold. Other approaches, such as the one by Kochurov et al. [21], simply set the curvature to a learnable parameter but do not account for the manifold changes in the Riemannian optimizers. This leads to hyperbolic vectors being updated with mismatched curvatures and others being inaccurately reprojected, resulting in instability and accuracy degradation. Additionally, some methods, like the one by Kim et al. [20], store all manifold parameters as Euclidean vectors and project them before use. While this approach partially mitigates the issue of mismatched curvature operations, it remains less accurate and more computationally expensive. In comparison, our proposed optimization schema maintains the parameters on the manifold and optimizes them directly by performing the necessary operations to transition between the variable curvature spaces.

**Metric Learning** Metric learning relies on the concept of structuring the distribution in the embedding space so that related data points are positioned closer together, while less related points

are placed further apart. To facilitate this process, numerous studies have introduced additional loss functions that explicitly encourage this behavior. Contrastive losses, for instance, operate on pairs of data points and propose a penalty that is proportional to the distances between negative pairs and inversely proportional to the distance between positive pairs [4]. Triplet loss extends this idea by considering sets of three points: an anchor, a positive sample, and a negative sample [39]. Instead of changing the distances between points absolutely, it ensures that the distance between the anchor and the positive sample is less than the distance between the anchor and the negative sample, plus a margin, thus enforcing a relational criterion.

These approaches have also been adapted to hierarchical problem settings under hyperbolic manifolds [20, 43]. Notably, Kim et al. [20] developed a method for learning continuous hierarchical representations using a deep learning, data-mining-like approach that relies on the innate relationships of the embeddings rather than their labels. They employ a proxy-based method that models the data on the Poincaré ball, facilitating a more natural extension to hierarchical tasks. Building on this, we extend the approach by modeling the loss function in the Lorentz manifold and incorporating a learnable curvature to better handle data with varying levels of hierarchy.

### 3 Methodology

#### 3.1 Background

The hyperbolic space is a Riemannian manifold with a constant negative sectional curvature  $c < 0$ . There are many conformal models of hyperbolic space but we focus our work on the hyperboloid, or Lorentz manifold. The  $n$ -dimensional Lorentz model  $\mathbb{L}_K^n = (\mathcal{L}^n, \mathfrak{g}_x^K)$  is defined with  $\mathcal{L}^n := \{\mathbf{x} \in \mathbb{R}^{n+1} \mid \langle \mathbf{x}, \mathbf{x} \rangle_{\mathcal{L}} = \frac{1}{K}, x_t > 0\}$  where  $\frac{-1}{K} = c$ , and with the Riemannian metric  $\mathfrak{g}_x^K = \text{diag}(-1, 1, \dots, 1)$ . This models the upper sheet of a two-sheeted hyperboloid centered at  $\bar{\mathbf{0}} = [\sqrt{K}, 0, \dots, 0]^T$ . We inherit the terminology of special relativity and refer to the first dimension of a Lorentzian vector as the time component  $x_t$  and the remainder of the vector, the space dimension  $\mathbf{x}_s$ . The Lorentzian inner product then becomes  $\langle \mathbf{x}, \mathbf{y} \rangle_{\mathcal{L}} := -x_t y_t + \mathbf{x}_s^T \mathbf{y}_s = \mathbf{x}^T \text{diag}(-1, 1, \dots, 1) \mathbf{y}$ . We now define the common hyperbolic operations in the Lorentz space.

**Distance** Distance in hyperbolic space is the magnitude of the geodesic forming the shortest path between two points. Let  $\mathbf{x}, \mathbf{y} \in \mathbb{L}_K^n$ , the distance between them is given by  $d_{\mathcal{L}}(\mathbf{x}, \mathbf{y}) = \sqrt{K} \cosh^{-1}(\frac{-\langle \mathbf{x}, \mathbf{y} \rangle_{\mathcal{L}}}{K})$ . We also define the square distance by Law et al. [23] as  $d_{\mathcal{L}}^2(\mathbf{x}, \mathbf{y}) = \|\mathbf{x} - \mathbf{y}\|_{\mathcal{L}}^2 = -2K - 2\langle \mathbf{x}, \mathbf{y} \rangle_{\mathcal{L}}$ .

**Exponential and Logarithmic Maps** Seeing as the Lorentz space is a Riemannian manifold, it is locally Euclidean. This can best be described through the tangent space  $\mathcal{T}_x \mathcal{M}$ , a first-order approximation of the manifold at a given point  $\mathbf{x}$ . The exponential map,  $\exp_x^K(\mathbf{z}) : \mathcal{T}_x \mathbb{L}_K^n \rightarrow \mathbb{L}_K^n$  is then the operation that maps a tangent vector  $\mathcal{T}_x \mathbb{L}_K^n$  onto the manifold through  $\exp_x^K(\mathbf{z}) = \cosh(\alpha) \mathbf{x} + \sinh(\alpha) \frac{\mathbf{z}}{\alpha}$ , with  $\alpha = \sqrt{1/K} \|\mathbf{z}\|_{\mathcal{L}}$ ,  $\|\mathbf{z}\|_{\mathcal{L}} = \sqrt{\langle \mathbf{z}, \mathbf{z} \rangle_{\mathcal{L}}}$ . The logarithmic map is the inverse of this mapping and can be described as  $\log_x^K(\mathbf{y}) = \frac{\cosh^{-1}(\beta)}{\sqrt{\beta^2 - 1}} \cdot (\mathbf{y} - \beta \mathbf{x})$ , with  $\beta = -\frac{1}{K} \langle \mathbf{x}, \mathbf{y} \rangle_{\mathcal{L}}$ .

**Parallel Transport** A parallel transport operation  $\text{PT}_{\mathbf{x} \rightarrow \mathbf{y}}^K(\mathbf{v})$  describes the mapping of a vector on the manifold  $\mathbf{v}$  from the tangent space of  $\mathbf{x} \in \mathbb{L}$  to the tangent space of  $\mathbf{y} \in \mathbb{L}$ . This operation is given as  $\text{PT}_{\mathbf{x} \rightarrow \mathbf{y}}^K(\mathbf{v}) = \mathbf{v} + \frac{\langle \mathbf{y}, \mathbf{v} \rangle_{\mathcal{L}}}{K - \langle \mathbf{x}, \mathbf{y} \rangle_{\mathcal{L}}} (\mathbf{x} + \mathbf{y})$ .

**Lorentzian Centroid [23]** Also denoted as  $\mu_{\mathbb{L}}$ , is the weighted centroid between points on the manifold based on the Lorentzian square distance. Given the weights  $\nu, \mu = \frac{\sum_{i=1}^m \nu_i \mathbf{x}_i}{\sqrt{1/K} \|\sum_{i=1}^m \nu_i \mathbf{x}_i\|_{\mathcal{L}}}$ .

#### 3.2 Riemannian Optimization

**Optimizers for Learned Curvatures** In their hyperbolic learning library GeoOpt, Kochurov et al. [21] attempt to make the curvature of the hyperbolic space a learnable parameter. However, we have found no further work that makes proper use of this feature. Additionally, our empirical tests

show that this approach often results in higher levels of instability and performance degradation. We attribute these issues to the naive implementation of curvature updates, which fails to incorporate the updated hyperbolic operations into the learning algorithm. Specifically, Riemannian optimizers rely on Riemannian projections of Euclidean gradients and projected momentums onto the tangent spaces of gradient vectors. These operations depend on the current properties of the manifold that houses the hyperbolic parameters being updated. From this, we can identify one main issue with the naive curvature learning approach.

The order in which parameters are updated is crucial. Specifically, if the curvature of the space is updated before the hyperbolic parameters, the Riemannian projections and tangent projections of the gradients and momentums become invalid. This happens because the projection operations start using the new curvature value, even though the hyperbolic parameters, hyperbolic gradients, and momentums have not yet been reprojected onto the new manifold.

To resolve this issue, we propose a projection schema and an ordered parameter update process. To sequentialize the optimization of model parameters, we first update all manifold and Euclidean parameters, and then update the curvatures after. Next, we parallel transport all Riemannian gradients and project all hyperbolic parameters to the tangent space at the origin using the old curvature value. Since this tangent space remains invariant when the manifold curvature changes, we can assume the points now lie on the tangent space of the new origin as well. We then re-project the hyperbolic tensors back onto the manifold using the new curvature value and parallel transport the Riemannian gradients to their respective parameters. This process can be illustrated in algorithm 1.

---

**Algorithm 1** Curvature Learning Aware Optimization

---

Given parameters  $\theta = [\theta_{euclid}, \theta_L, \theta_k]$  and gradients denoted  $\mathcal{G}$

**procedure** OPTIMIZER STEP( $\theta$ )

**for**  $p$  in  $\theta_{euclid} \cup \theta_L$  **do**

    Vanilla Riemannian Optimizer Step

**end for**

**for**  $p$  in  $\theta_k$  **do**

    Vanilla Riemannian Optimizer Step

**end for**

  MoveParameters()

**end procedure**

**procedure** MOVE PARAMETERS

**for**  $p$  in  $\theta_L$  **do**

$\mathcal{G}_{temp} = \mathcal{G} + \frac{\langle \bar{\mathbf{0}}_{t-1}, \mathcal{G} \rangle_{\mathcal{L}}}{K_{t-1} - \langle p, \bar{\mathbf{0}}_{t-1} \rangle_{\mathcal{L}}} (p + \bar{\mathbf{0}}_{t-1}) \rightarrow \text{PT}_{p \rightarrow \bar{\mathbf{0}}_{t-1}}^{K_{t-1}}(\mathcal{G})$

$z = \frac{\cosh^{-1}(\beta)}{\sqrt{\beta^2 - 1}} \cdot (p - \beta \bar{\mathbf{0}}_{t-1})$ , with  $\beta = \frac{-1}{K_{t-1}} \langle \bar{\mathbf{0}}_{t-1}, p \rangle_{\mathcal{L}} \rightarrow \log_{\bar{\mathbf{0}}_{t-1}}^{K_{t-1}}(p)$

$p = \frac{1}{\sqrt{1/K_t}} \left[ \cosh(\sqrt{1/K_t} \|z\|), \sinh(\sqrt{1/K_t} \|z\|) \frac{z}{\|z\|} \right] \rightarrow \exp_{\bar{\mathbf{0}}_{t-1}}^{K_t}(z)$

$\mathcal{G} = \mathcal{G}_{temp} + \frac{\langle p, \mathcal{G}_{temp} \rangle_{\mathcal{L}}}{K_t - \langle p, \bar{\mathbf{0}}_t \rangle_{\mathcal{L}}} (p + \bar{\mathbf{0}}_t) \rightarrow \text{PT}_{\bar{\mathbf{0}}_t \rightarrow p}^K(\mathcal{G}_{temp})$

**end for**

**end procedure**

---

**Riemannian AdamW Optimizer** Recent works, especially with transformers, rely on the AdamW optimizer proposed by Loshchilov and Hutter [26] for training. As of current, there is no established Riemannian variant of this optimizer. We attempt to derive AdamW for the Lorentz manifold and argue a similar approach could be generalized for the Poincaré ball. The main difference between AdamW and Adam is the direct weight regularization which is more difficult to perform in the Lorentz space given the lack of an intuitive subtraction operation on the manifold. To resolve this, we model the regularized parameter instead as a weighted centroid with the origin. The regularization schema becomes:

$$\theta_t = \begin{cases} \mu_L([\theta_{t-1}, \bar{\mathbf{0}}], \nu = \mathbf{W}) & \text{if } \theta \in \mathbb{L} \\ \theta_{t-1} - \gamma \theta_{t-1} \lambda & \text{otherwise} \end{cases}$$

where  $\gamma$  is the learning rate,  $\lambda$  is the weight decay value, and  $\mathbf{W} = [1 - \gamma\lambda, \gamma\lambda]$ . By removing the later gradient decay and introducing this operation, we adapt AdamW for use in the Lorentz space.

**Maximum Distance Rescaling** Vectors in the hyperboloid models can be defined as  $\mathbf{x} = [x_t, \mathbf{x}_s]^T \in \mathbb{L}_K^n$  where  $x_t = \sqrt{\|\mathbf{x}_s\|^2 + K}$ ,  $K = -1/c$  and  $c$  is the manifold curvature. As such, Lorentzian projections and operations rely on the ability to accurately calculate the corresponding time component  $x_t$  for the hyperbolic vectors. Under Float64 precision, Mishne et al. [28] derive a maximum value for the time component  $x_{t_{max}} = 10^8$ . Values above this push vectors off the Lorentz manifold and onto the cone defined by  $x_t^2 = \sum \mathbf{x}_s^2$ . This is because  $\|\mathbf{x}_s\|^2 + K$  is then approximated as  $\|\mathbf{x}_s\|^2$ . Based on the above, and given a specific  $K$ , we can derive a maximum representational radius for the model as

$$D(x, \bar{\mathbf{0}})_{max}^K = \text{arccosh}\left(\frac{x_{t_{max}}}{\sqrt{K}}\right) \cdot \sqrt{K} \quad (1)$$

Under Float32 precision, and to account for values of  $K < 1$  we use a limit value of  $x_{t_{max}} = 2 \cdot 10^3$ . When projected onto the tangent space of the origin, and with  $K = 1$ , this translates to  $\|\log_{\bar{\mathbf{0}}}^1(\mathbf{x})\| = D(x, \bar{\mathbf{0}})_{max}^1 = 9.1$ . This value changes considerably as the value of  $K$  changes. Vectors outside this radius lead to instability and performance degradation due to inaccurate approximation. This problem is only exacerbated as the dimensionality of the hyperbolic vector increases. Higher dimensional vectors tend to have larger norms which limits hyperbolic models' abilities to scale up.

As such, we propose a maximum distance rescaling function on the tangent of the origin to conform with the representational capacity of hyperbolic manifolds.

$$\mathbf{x}_{rescaled} = \exp_{\bar{\mathbf{0}}}^K \left( \mathbf{z} \cdot \frac{D(x, \bar{\mathbf{0}})_{max}^k \cdot \tanh(r \cdot \|\mathbf{z}\|)}{\|\mathbf{z}\|} \right) \quad (2)$$

where

$$r = \text{atanh}\left(\frac{0.99}{s \cdot D(x, \bar{\mathbf{0}})_{max}^k}\right), \text{ and } \mathbf{z} = \log_{\bar{\mathbf{0}}}^K(\mathbf{x}) \quad (3)$$

and  $s$  is a tightness factor. That controls the scaling intensity as can be seen through  $\lim_{\|\mathbf{z}\| \rightarrow s \cdot D_{0_{max}}^k} (\|\mathbf{z}\|_{rescaled}) = D_{0_{max}}^k$ .

Specifically, we apply it when moving parameters across different manifolds. This includes moving from the Euclidean space to the Lorentz space and moving between Lorentz spaces of different curvatures. We also apply the scaling after Lorentz Boosts and direct Lorentz concatenations [31]. Additionally, we add this operation after the variance-based rescaling in the batchnorm layer. This is because we run into situations where adjusting to the variance pushes the points outside the radius during the operation.

### 3.3 Towards Efficient Architectural Components

**Lorentz Convolutional Layer** In their work, Bdeir et al. [1] relied on dissecting the convolution operation into a window-unfolding followed by a modified version of the Lorentz Linear layer by Chen et al. [3]. However, an alternative definition for the Lorentz Linear layer is offered by Dai et al. [5] based on a direct decomposition of the operation into a Lorentz boost and a Lorentz rotation. We follow the dissection scheme by Bdeir et al. [1] but rely on Dai et al. [5]'s alternate definition of the Lorentz linear transformation. The core transition here would be moving from a matrix multiplication on the spatial dimensions followed by a reprojection, to learning an individual rotation operation and a Lorentz Boost.

Here the rotation relies on optimizing a parameterized matrix  $\hat{\mathbf{W}} \in \mathbb{S}$ . Where

$$\mathbb{S}(n', n) = \mathbf{M} \in \mathbb{R}^{(n' \cdot n)} : \mathbf{M}^T \mathbf{M} = \mathbf{I} \quad (4)$$

is the Stiefel manifold. It is important to note that  $n \leq n'$  ensures that the weight matrix columns are orthogonal which then preserves the norms along the rows of the multiplied input. In the case of the convolution operation, and after the initial unfolding,  $n$  and  $n'$  correspond to

( $channels_{in} \cdot kernel_{width} \cdot kernel_{height}$ ) and  $channels_{out}$  respectively. Here we can see that the condition for orthogonal columns is not always fulfilled. As such, for  $n > n'$  we rely on the norm-preserving transformation  $z = \mathbf{W}^T \mathbf{x} \cdot \frac{\|\mathbf{x}\|}{\|\mathbf{W}^T \mathbf{x}\|}$  where  $\mathbf{W} \in \mathbb{R}^{(n' \cdot n)}$ . Given the above formulations, we are able to use the existing efficient implementations of the convolution operation by a direct parameterization of the kernel weights. Finally, we formalize the new Lorentz Convolution as:

$$out = \text{LorentzBoost}(\text{TanhScaling}(\text{RotationConvolution}(x))) \quad (5)$$

where `TanhRescaling` is the operation described in 2 and `RotationConvolution` is a normal convolution parameterized through the procedure in 2, where `Orthogonalize` is a Cayley transformation similar to [16]. We use the Cayley transformation in particular because it always results in an orthonormal matrix with a positive determinant which prevents the rotated point from being carried to the lower sheet of the hyperboloid.

---

**Algorithm 2** Lorentz Convolution Parameterization

---

```

 $\mathbf{W} \in \mathbb{R}^{C_{in}, C_{out}, K_{width}, K_{length}}$ 
procedure ADAPTWEIGHT( $\mathbf{W}$ )
  if  $K_{width} \cdot K_{length} \cdot C_{in} > C_{out}$  then
    return  $\mathbf{W}$ 
  else
     $\mathbf{W} = \mathbf{W}.\text{reshape}(K_{width} \cdot K_{length} \cdot C_{in}, C_{out})$ 
     $\hat{\mathbf{W}}_{core} = \text{Orthogonalize}(\mathbf{W})$ 
    return  $\hat{\mathbf{W}}.\text{reshape}(C_{in}, C_{out}, K_{width}, K_{length})$ 
  end if
end procedure

```

---

$\hat{\mathbf{W}}_{core}$  can also be learned directly on the SPD manifold similar to Dai et al. [5]. This definition of the convolution operation allows to use the existing efficient implementations of 2D convolutions, saving both memory and runtime.

**Lorentz-Core Bottleneck Block** In an effort to expand on the idea of hybrid hyperbolic encoders [1], we designed the Lorentz Core Bottleneck blocks for Hyperbolic Resnet-based models. This is similar to a standard Euclidean bottleneck block except we replace the internal 3x3 convolutional layer with our efficient convolutional layer as seen in figure 1. We are then able to benefit from a hyperbolic structuring of the embeddings in each block while maintaining the flexibility and speed of Euclidean models. We interpret this integration as a form of hyperbolic bias that can be adopted into Resnets without strict hyperbolic modeling.

## 4 Experiments

### 4.1 Hierarchical Metric Learning Problem

In their paper Kim et al. [20] take on the problem of hierarchical clustering using an unsupervised hyperbolic loss regularizer they name HIER. This method relies on the use of hierarchical proxies as learnable ancestors of the embedded data points in hyperbolic space. Given a triplet of points  $x_i, x_j, x_k$  where  $x_i$  and  $x_j$  are determined to be related by a reciprocal nearest neighbor measure, and  $x_k$  is an unrelated point, the HIER loss regularizer is then calculated as

$$\begin{aligned} \mathcal{L}_{\text{HIER}}(t) = & [d_B(x_i, \rho_{ij}) - d_B(x_i, \rho_{ijk}) + \delta]_+ \\ & + [d_B(x_j, \rho_{ij}) - d_B(x_j, \rho_{ijk}) + \delta]_+ \\ & + [d_B(x_k, \rho_{ijk}) - d_B(x_k, \rho_{ij}) + \delta]_+, \end{aligned} \quad (6)$$

where  $d_B$  denotes the hyperbolic distance on the Poincaré ball. This encourages a smaller hyperbolic distance between  $x_i, x_j$ , and  $\rho_{ij}$ , and a larger distance with  $\rho_{ijk}$ . The opposite signal is then applied in the case of  $x_k$ , the irrelevant data point. Kim et al. [20] show substantial performance uplifts for the HIER loss when applied to a variety of network architectures.

In the following experiment, we extend HIER to the Lorentz model (LHIER) and compare against the results provided by [20]. The aim of this is proving the effectiveness of our Lorentzian AdamW optimizer, general optimization scheme, curvature learning, and max distance scaling.

**Experimental Setup** We follow the experimental setup in Kim et al. [20] and rely on four main datasets: CUB-200-2011 (CUB)[42], Cars-196 (Cars)[22], Stanford Online Product (SOP)[34], and In-shop Clothes Retrieval (InShop)[24]. Performance is measured using Recall@k which is the fraction of queries with one or more relevant samples in their k-nearest neighbors. Additionally, all model backbones are pretrained on Imagenet to ensure fair comparisons with the previous work.

**Moving to Lorentz Space** We adapt the HIER to the hyperboloid using three major changes. We first replace the Euclidean linear layer with a Lorentzian linear layer in the model neck and implement our max distance scaling operation after. We then set the hierarchical proxies as learnable hyperbolic parameters and optimize them directly on the manifold using our Lorentzian AdamW. Finally, we change the Poincaré distance to the Lorentz distance for the LHIER loss and set the hierarchical proxies to be scaled beforehand. We also continue to use on fp16 precision which shows our model is more robust to stability and imprecision issues.

**Results** As show in table 1, our HIER+ model manages to improve performance in almost all scenarios. However, the percentage change varies depending on the dataset and the model used. While we do the best in the case of Resnet models, we are particularly worse for the DeiT model, especially at the higher dimensionality where our method is out performed in most datasets by HIER. This could be the issue of a lack of hyperparameter tuning, specifically in the case of the tanh scaling; the  $s$  factor which controls the tightness of the outputs. Kim et al. [20] control this through the use of norm clipping with varying intensities, a similar approach could be adopted to study the best-fitting scaling factors given the experimental settings.

## 4.2 Standard Classification Problem

**Experimental Setup** We follow the experimental setup of Bdeir et al. [1] and rely on three main datasets: CIFAR10, CIFAR100, Mini-Imagenet. We also extend the experiments to include Resnet50, however, due to the increased memory cost, we are only able to compare to the base Euclidean counterpart and hybrid models. For the Resnet-18 models we do no use our Lorentz core blocks and instead recreate the hybrid encoder similar to Bdeir et al. [1]. For all models, we use the efficient convolutional layer, all hyperbolic vectors are scaled using our max distance rescaling with  $s = 2$ . Additionally, curvature learning is performed for both our Resnet-18 and Resnet-50 using Riemannian SGD with our fixed schema. Encoder and decoder manifolds are separated with each capable of learning its own curvature for better flexibility.

**Results** For Resnet-18 tests, we see in table 2 that the new architectures perform better in all scenarios. The smallest performance was mainly seen between the hybrid models, this could generally be because the hyperbolic bias played by the additional hyperbolic components is not as prominent as in a fully hyperbolic model. This could lead to the model benefiting less from the proposed changes. We can verify this through the bigger gap in performance between the fully hyperbolic models where our proposed model sees a 74% lift in accuracy and even matches the hybrid encoders in this scenario. To study this we looked at the new curvature learned by the encoder and found that it tended towards approximately -0.6 resulting in a flatter manifold.

As for the Resnet-50 tests, we see in table 3, that HECNN+ is now able to greatly outperform the Euclidean model across all datasets as well. Even in the case of Tiny-Imagenet where other model accuracies begin to break down. This is probably due to the more fluid integration of hyperbolic elements and the extensive scaling to help deal with higher dimensional embeddings.

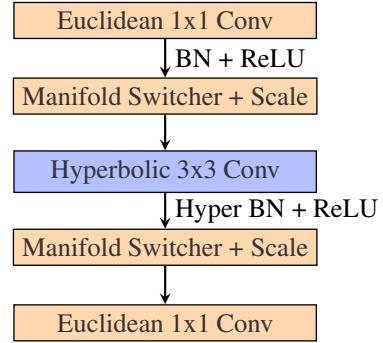


Figure 1: Lorentz-Core Bottleneck block replaces the internal 3x3 Euclidean convolution with the corresponding hyperbolic operations

Table 1: Performance of metric learning methods on the four datasets as provided by [20]. All architecture backbones are pretrained and tested with the new LHIER loss. Superscripts denote their embedding dimensions and † indicates models using larger input images. As in [20], network architectures are abbreviated as, R–ResNet50 [15], B–Inception with BatchNorm [17], De–DeiT [37], DN–DINO [2] and V–ViT [7]

Methods	Arch.	CUB			Cars			SOP			In-Shop		
		R@1	R@2	R@4	R@1	R@2	R@4	R@1	R@10	R@100R@1	R@10	R@20	
<i>Backbone architecture: CNN</i>													
NSoftmax [44]	R <sup>128</sup>	56.5	69.6	79.9	81.6	88.7	93.4	75.2	88.7	95.2	86.6	96.8	97.8
MIC [33]	R <sup>128</sup>	66.1	76.8	85.6	82.6	89.1	93.2	77.2	89.4	94.6	88.2	97.0	-
XBM [41]	R <sup>128</sup>	-	-	-	-	-	-	80.6	91.6	96.2	91.3	97.8	98.4
XBM [41]	B <sup>512</sup>	65.8	75.9	84.0	82.0	88.7	93.1	79.5	90.8	96.1	89.9	97.6	98.4
HTL [11]	B <sup>512</sup>	57.1	68.8	78.7	81.4	88.0	92.7	74.8	88.3	94.8	80.9	94.3	95.8
MS [40]	B <sup>512</sup>	65.7	77.0	86.3	84.1	90.4	94.0	78.2	90.5	96.0	89.7	97.9	98.5
SoftTriple [30]	B <sup>512</sup>	65.4	76.4	84.5	84.5	90.7	94.5	78.6	86.6	91.8	-	-	-
PA [19]	B <sup>512</sup>	68.4	79.2	86.8	86.1	91.7	95.0	79.1	90.8	96.2	91.5	98.1	98.8
NSoftmax [44]	R <sup>512</sup>	61.3	73.9	83.5	84.2	90.4	94.4	78.2	90.6	96.2	86.6	97.5	98.4
†ProxyNCA++ [33]	B <sup>512</sup>	69.0	79.8	87.3	86.5	92.5	95.7	80.7	92.0	96.7	90.4	98.1	98.8
Hyp [9]	R <sup>512</sup>	65.5	76.2	84.9	81.9	88.8	93.1	79.9	91.5	96.5	90.1	98.0	98.7
HIER [20]	R <sup>512</sup>	70.1	79.4	86.9	88.2	93.0	95.6	80.2	91.5	96.6	92.4	98.2	98.8
LHIER (ours)	R <sup>512</sup>	71.0	80.3	87.8	88.7	93.2	95.7	81.3	92.1	96.8	92.8	98.5	99.0
<i>Backbone architecture: ViT</i>													
IRT <sub>R</sub> [8]	De <sup>128</sup>	72.6	81.9	88.7	-	-	-	83.4	93.0	97.0	91.1	98.1	98.6
Hyp [9]	De <sup>128</sup>	74.7	84.5	90.1	82.1	89.1	93.4	83.0	93.4	97.5	90.9	97.9	98.6
HIER [20]	De <sup>128</sup>	75.2	84.2	90.0	85.1	91.1	95.1	82.5	92.7	97.0	91.0	98.0	98.6
LHIER (ours)	De <sup>128</sup>	75.5	84.7	90.6	85.4	91.7	95.6	82.7	93.5	97.4	91.4	98.5	98.9
Hyp [9]	DN <sup>128</sup>	78.3	86.0	91.2	86.0	91.9	95.2	84.6	94.1	97.7	92.6	98.4	99.0
HIER [20]	DN <sup>128</sup>	78.5	86.7	91.5	88.4	93.3	95.9	84.9	94.2	97.5	92.6	98.4	98.9
LHIER (ours)	DN <sup>128</sup>	78.8	87.0	91.9	88.9	93.2	96.4	85.1	94.9	98.2	92.7	98.5	99.0
Hyp [9]	V <sup>128</sup>	84.0	90.2	94.2	82.7	89.7	93.9	85.5	94.9	98.1	92.7	98.4	98.9
HIER [20]	V <sup>128</sup>	84.2	90.1	93.7	86.4	91.9	95.1	85.6	94.6	97.8	92.7	98.4	98.9
LHIER (ours)	V <sup>128</sup>	84.6	90.2	93.9	86.7	92.0	95.3	85.9	95.0	98.0	92.8	98.4	99.0
IRT <sub>R</sub> [8]	De <sup>384</sup>	76.6	85.0	91.1	-	-	-	84.2	93.7	97.3	91.9	98.1	98.9
DeiT-S [37]	De <sup>384</sup>	70.6	81.3	88.7	52.8	65.1	76.2	58.3	73.9	85.9	37.9	64.7	72.1
Hyp [9]	De <sup>384</sup>	77.8	86.6	91.9	86.4	92.2	95.5	83.3	93.5	97.4	90.5	97.8	98.5
HIER [20]	De <sup>384</sup>	78.7	86.8	92.0	88.9	93.9	96.6	83.0	93.1	97.2	90.6	98.1	98.6
LHIER (ours)	De <sup>384</sup>	78.3	86.2	91.8	88.7	93.4	96.4	82.8	92.9	96.9	91.0	98.2	98.7
DINO [2]	DN <sup>384</sup>	70.8	81.1	88.8	42.9	53.9	64.2	63.4	78.1	88.3	46.1	71.1	77.5
Hyp [9]	DN <sup>384</sup>	80.9	87.6	92.4	89.2	94.1	96.7	85.1	94.4	97.8	92.4	98.4	98.9
HIER [20]	DN <sup>384</sup>	81.1	88.2	93.3	91.3	95.2	97.1	85.7	94.6	97.8	92.5	98.6	99.0
LHIER (ours)	DN <sup>384</sup>	81.3	88.4	93.3	91.5	95.1	97.6	85.9	95.0	98.1	92.7	98.5	98.9
ViT-S [7]	V <sup>384</sup>	83.1	90.4	94.4	47.8	60.2	72.2	62.1	77.7	89.0	43.2	70.2	76.7
Hyp [9]	V <sup>384</sup>	85.6	91.4	94.8	86.5	92.1	95.3	85.9	94.9	98.1	92.5	98.3	98.8
HIER [20]	V <sup>384</sup>	85.7	91.3	94.4	88.3	93.2	96.1	86.1	95.0	98.0	92.8	98.4	99.0
LHIER (ours)	V <sup>384</sup>	86.2	92.1	95.2	88.6	93.6	96.3	86.7	95.3	98.3	92.9	98.5	99.0

**Ablation** We test the effect of individual model components in table 5. Each subsequent model involves the default architecture presented in the experimental setup minus the mentioned component. As we can see, the best results are achieved when all the architectural components are included. In the case of attempting to learn the curvature without the proposed optimizer schema, the model breaks completely down due to excessive numerical inaccuracies. One other benefit that we find from learning the curvature is quicker convergence. The model is able to reach convergence in 130 epochs vs the 200 epochs required by a static curve model.

Table 4: Computation requirements of different convolution types for HECNN+ on CIFAR-100 and a batch size of 80.

	Vmem(GB)	Runtime(s/epoch)
Euclidean	4.5	30
HECNN+ - [1]	15.6	300
HECNN+ - Ours	8.1	100



Table 2: Classification accuracy (%) of ResNet-18 models. We estimate the mean and standard deviation from five runs. The best performance is highlighted in bold (higher is better).

	CIFAR-10 ( $\delta_{rel} = 0.26$ )	CIFAR-100 ( $\delta_{rel} = 0.23$ )	Tiny-ImageNet ( $\delta_{rel} = 0.20$ )
Euclidean [15]	95.14 $\pm$ 0.12	77.72 $\pm$ 0.15	65.19 $\pm$ 0.12
Hybrid Poincaré [14]	95.04 $\pm$ 0.13	77.19 $\pm$ 0.50	64.93 $\pm$ 0.38
Hybrid Lorentz [1]	94.98 $\pm$ 0.12	78.03 $\pm$ 0.21	65.63 $\pm$ 0.10
Poincaré ResNet [38]	94.51 $\pm$ 0.15	76.60 $\pm$ 0.32	62.01 $\pm$ 0.56
HECNN Lorentz [1]	95.16 $\pm$ 0.11	78.76 $\pm$ 0.24	65.96 $\pm$ 0.18
HECNN+ (ours)	95.15 $\pm$ 0.07	78.80 $\pm$ 0.12	65.98 $\pm$ 0.11
HCNN Lorentz [1]	95.15 $\pm$ 0.08	78.07 $\pm$ 0.17	65.71 $\pm$ 0.13
HCNN+ (ours)	95.17 $\pm$ 0.09	<b>78.81<math>\pm</math>0.19</b>	<b>66.12<math>\pm</math>0.14</b>

Table 3: Classification accuracy (%) of ResNet-50 models. The best performance is highlighted in bold (higher is better).

	CIFAR-10 ( $\delta_{rel} = 0.26$ )	CIFAR-100 ( $\delta_{rel} = 0.23$ )	Tiny-ImageNet ( $\delta_{rel} = 0.20$ )
Euclidean [15]	95.14	78.52	66.23
Hybrid Lorentz [1]	95.38	79.35	66.01
HECNN [1]	95.42	79.83	66.30
HECNN+ (ours)	<b>95.46</b>	<b>80.86</b>	<b>67.18</b>

We then study the effectiveness of our efficient convolution in table 4. We see a  $\sim 48\%$  reduction in memory usage and  $\sim 66\%$  reduction in runtime. We attribute this improvement to the efficient closed-source convolution operations we can now leverage. However, there is still much room for improvement compared to the euclidean model. We identify the batchnorm operation as the new memory and runtime bottleneck accounting for around 60% of the runtime and around 30% of the memory. Factorizing the many parallel transports and tangent mappings required for this operation would be

Table 5: Ablation experiments for Resnet-50 models on Cifar-100.

	CIFAR-100
HECNN+ - Default	<b>80.86</b>
HECNN+ - fixed curve	79.6
HECNN+ - no scaling	80.13
HECNN+ - no optim scheme	<i>NaaN</i>

the next step in mitigating this issue.

## 5 Conclusion

In our work, we present many new components and schemas for the use of hyperbolic deep learning in hyperbolic vision. We present a new optimizer schema that allows for curvature learning, a tanh scaling to prevent numerical precision issues, a Riemannian Adam Optimizer, and efficient formulations of existing convolutional operations. We test these components in two different problem scenarios, hierarchical metric learning and classification, and prove the potential of these new components even in float16 conditions which are notoriously unstable for hyperbolic models.

However, there is still much progress to be made. The scaling operations provide a general method of keeping the embeddings within the representative radius but it could also be used for norm clipping. A study has to be done on the effect of embedding bounding for hyperbolic models as it has shown to be beneficial before [14, 20]. Additionally, more efficiency can still be gained from hyperbolic models through further optimizations to the batch normalization layers. Finally, there is still the issue of the hyperbolic feedforward layer when going from higher to lower dimensionality. We currently match norms to ensure a rotation operation but we encourage finding alternate approaches that are better conforming to the manifold mathematics.

## References

- [1] A. Bdeir, K. Schwethelm, and N. Landwehr. Fully hyperbolic convolutional neural networks for computer vision, 2024.
- [2] M. Caron, H. Touvron, I. Misra, H. Jégou, J. Mairal, P. Bojanowski, and A. Joulin. Emerging properties in self-supervised vision transformers. In *Proc. IEEE International Conference on Computer Vision (ICCV)*, 2021.
- [3] W. Chen, X. Han, Y. Lin, H. Zhao, Z. Liu, P. Li, M. Sun, and J. Zhou. Fully hyperbolic neural networks, 2022.
- [4] S. Chopra, R. Hadsell, and Y. LeCun. Learning a similarity metric discriminatively, with application to face verification. In *Proc. IEEE Conference on Computer Vision and Pattern Recognition (CVPR)*, 2005.
- [5] J. Dai, Y. Wu, Z. Gao, and Y. Jia. A hyperbolic-to-hyperbolic graph convolutional network, 2021.
- [6] B. Dhingra, C. J. Shallue, M. Norouzi, A. M. Dai, and G. E. Dahl. Embedding text in hyperbolic spaces, 2018.
- [7] A. Dosovitskiy, L. Beyer, A. Kolesnikov, D. Weissenborn, X. Zhai, T. Unterthiner, M. Dehghani, M. Minderer, G. Heigold, S. Gelly, et al. An image is worth 16x16 words: Transformers for image recognition at scale. In *Proc. International Conference on Learning Representations (ICLR)*, 2021.
- [8] A. El-Nouby, N. Neverova, I. Laptev, and H. Jégou. Training vision transformers for image retrieval. *arXiv preprint arXiv:2102.05644*, 2021.
- [9] A. Ermolov, L. Mirvakhabova, V. Khrulkov, N. Sebe, and I. Oseledets. Hyperbolic vision transformers: Combining improvements in metric learning. In *Proc. IEEE Conference on Computer Vision and Pattern Recognition (CVPR)*, 2022.
- [10] O. Ganea, G. Becigneul, and T. Hofmann. Hyperbolic neural networks. In S. Bengio, H. Wallach, H. Larochelle, K. Grauman, N. Cesa-Bianchi, and R. Garnett, editors, *Advances in Neural Information Processing Systems*, volume 31. Curran Associates, Inc., 2018. URL <https://proceedings.neurips.cc/paper/2018/file/dbab2adc8f9d078009ee3fa810bea142-Paper.pdf>.
- [11] W. Ge, W. Huang, D. Dong, and M. R. Scott. Deep metric learning with hierarchical triplet loss. In *Proc. European Conference on Computer Vision (ECCV)*, 2018.
- [12] F. D. Giovanni, G. Luise, and M. Bronstein. Heterogeneous manifolds for curvature-aware graph embedding, 2022.
- [13] A. Gu, F. Sala, B. Gunel, and C. Ré. Learning mixed-curvature representations in product spaces. In *International Conference on Learning Representations*, 2018. URL <https://api.semanticscholar.org/CorpusID:108328651>.
- [14] Y. Guo, X. Wang, Y. Chen, and S. X. Yu. Clipped hyperbolic classifiers are super-hyperbolic classifiers. In *2022 IEEE/CVF Conference on Computer Vision and Pattern Recognition (CVPR)*, pages 1–10, Los Alamitos, CA, USA, jun 2022. IEEE Computer Society. doi: 10.1109/CVPR52688.2022.00010. URL <https://doi.ieeecomputersociety.org/10.1109/CVPR52688.2022.00010>.
- [15] K. He, X. Zhang, S. Ren, and J. Sun. Deep residual learning for image recognition. In *Proc. IEEE Conference on Computer Vision and Pattern Recognition (CVPR)*, June 2016.
- [16] K. Helfrich, D. Willmott, and Q. Ye. Orthogonal recurrent neural networks with scaled cayley transform, 2018.
- [17] S. Ioffe and C. Szegedy. Batch normalization: Accelerating deep network training by reducing internal covariate shift. In *Proc. International Conference on Machine Learning (ICML)*, 2015.
- [18] V. Khrulkov, L. Mirvakhabova, E. Ustinova, I. Oseledets, and V. Lempitsky. Hyperbolic image embeddings. In *Proc. IEEE Conference on Computer Vision and Pattern Recognition (CVPR)*, 2020.
- [19] S. Kim, D. Kim, M. Cho, and S. Kwak. Proxy anchor loss for deep metric learning. In *Proc. IEEE Conference on Computer Vision and Pattern Recognition (CVPR)*, 2020.
- [20] S. Kim, B. Jeong, and S. Kwak. Hier: Metric learning beyond class labels via hierarchical regularization, 2023.
- [21] M. Kochurov, R. Karimov, and S. Kozlukov. Geoopt: Riemannian optimization in pytorch, 2020.

- [22] J. Krause, M. Stark, J. Deng, and L. Fei-Fei. 3d object representations for fine-grained categorization. In *Proceedings of the IEEE International Conference on Computer Vision Workshops*, pages 554–561, 2013.
- [23] M. Law, R. Liao, J. Snell, and R. Zemel. Lorentzian distance learning for hyperbolic representations. In K. Chaudhuri and R. Salakhutdinov, editors, *Proceedings of the 36th International Conference on Machine Learning*, volume 97 of *Proceedings of Machine Learning Research*, pages 3672–3681. PMLR, 09–15 Jun 2019. URL <https://proceedings.mlr.press/v97/law19a.html>.
- [24] S. Liu, X. Qi, J. Shi, H. Zhang, and J. Jia. Multi-scale patch aggregation (MPA) for simultaneous detection and segmentation. In *Proc. IEEE Conference on Computer Vision and Pattern Recognition (CVPR)*, 2016.
- [25] S. Liu, J. Chen, L. Pan, C.-W. Ngo, T.-S. Chua, and Y.-G. Jiang. Hyperbolic visual embedding learning for zero-shot recognition. In *2020 IEEE/CVF Conference on Computer Vision and Pattern Recognition (CVPR)*, pages 9270–9278, 2020. doi: 10.1109/CVPR42600.2020.00929.
- [26] I. Loshchilov and F. Hutter. Decoupled weight decay regularization, 2019.
- [27] P. Mettes, M. G. Atigh, M. Keller-Ressel, J. Gu, and S. Yeung. Hyperbolic deep learning in computer vision: A survey, 2023.
- [28] G. Mishne, Z. Wan, Y. Wang, and S. Yang. The numerical stability of hyperbolic representation learning, 2022. URL <https://arxiv.org/abs/2211.00181>.
- [29] Y. Nagano, S. Yamaguchi, Y. Fujita, and M. Koyama. A wrapped normal distribution on hyperbolic space for gradient-based learning, 2019. URL <https://arxiv.org/abs/1902.02992>.
- [30] Q. Qian, L. Shang, B. Sun, J. Hu, H. Li, and R. Jin. Softtriple loss: Deep metric learning without triplet sampling. In *Proc. IEEE International Conference on Computer Vision (ICCV)*, 2019.
- [31] E. Qu and D. Zou. Lorentzian fully hyperbolic generative adversarial network, 2022. URL <https://arxiv.org/abs/2201.12825>.
- [32] E. Qu and D. Zou. Hyperbolic convolution via kernel point aggregation, 2023.
- [33] K. Roth, B. Brattoli, and B. Ommer. Mic: Mining interclass characteristics for improved metric learning. In *Proc. IEEE International Conference on Computer Vision (ICCV)*, 2019.
- [34] H. O. Song, Y. Xiang, S. Jegelka, and S. Savarese. Deep metric learning via lifted structured feature embedding. In *Proc. IEEE Conference on Computer Vision and Pattern Recognition (CVPR)*, 2016.
- [35] E. W. Teh, T. DeVries, and G. W. Taylor. Proxynca++: Revisiting and revitalizing proxy neighborhood component analysis. In *European Conference on Computer Vision (ECCV)*. Springer, 2020.
- [36] A. Tifrea, G. Bécigneul, and O.-E. Ganea. Poincaré glove: Hyperbolic word embeddings, 2018.
- [37] H. Touvron, M. Cord, M. Douze, F. Massa, A. Sablayrolles, and H. Jégou. Training data-efficient image transformers & distillation through attention. In *Proc. International Conference on Machine Learning (ICML)*, 2021.
- [38] M. van Spengler, E. Berkhout, and P. Mettes. Poincaré resnet, 2023.
- [39] J. Wang, Y. Song, T. Leung, C. Rosenberg, J. Wang, J. Philbin, B. Chen, and Y. Wu. Learning fine-grained image similarity with deep ranking. In *Proc. IEEE Conference on Computer Vision and Pattern Recognition (CVPR)*, 2014.
- [40] X. Wang, X. Han, W. Huang, D. Dong, and M. R. Scott. Multi-similarity loss with general pair weighting for deep metric learning. In *Proc. IEEE Conference on Computer Vision and Pattern Recognition (CVPR)*, 2019.
- [41] X. Wang, H. Zhang, W. Huang, and M. R. Scott. Cross-batch memory for embedding learning. In *Proc. IEEE Conference on Computer Vision and Pattern Recognition (CVPR)*, pages 6388–6397, 2020.
- [42] P. Welinder, S. Branson, T. Mita, C. Wah, F. Schroff, S. Belongie, and P. Perona. Caltech-UCSD Birds 200. Technical Report CNS-TR-2010-001, California Institute of Technology, 2010.
- [43] Z. Yang, M. Bastan, X. Zhu, D. Gray, and D. Samaras. Hierarchical proxy-based loss for deep metric learning. 2022.
- [44] A. Zhai and H.-Y. Wu. Classification is a strong baseline for deep metric learning. *arXiv preprint arXiv:1811.12649*, 2018.
- [45] Y. Zhu, D. Zhou, J. Xiao, X. Jiang, X. Chen, and Q. Liu. Hypertext: Endowing fasttext with hyperbolic geometry, 2021.